Available online at www.sciencedirect.com

SciVerse ScienceDirect

Ceramics International 38 (2012) 3111–3120

CERAMICS INTERNATIONAL

www.elsevier.com/locate/ceramint

Prediction total specific pore volume of geopolymers produced from waste ashes by ANFIS

Ali Nazari [a,*], Gholamreza Khalaj [a], Shadi Riahi [a], Hamid Bohlooli [b], Mohammad Mehdi Kaykha [c]

[a] Department of Materials Engineering, Science and Research Branch, Islamic Azad University, Tehran, Iran
[b] Department of Mechanical Engineering, Birjand Branch, Islamic Azad University, Birjand, Iran
[c] Young Researchers Club, Birjand Branch, Islamic Azad University, Birjand, Iran

Received 9 June 2011; received in revised form 2 December 2011; accepted 6 December 2011
Available online 16 December 2011

Abstract

In the present work, total specific pore volume of geopolymers which made from a mixture of fly ash and rice husk bark ash has been predicted by adaptive network-based fuzzy inference systems (ANFIS). Different specimens were subjected to porosimetry tests at 7 and 28 days of curing. One set of the specimens were water cured at room temperature until reaching to 7 and 28 days and the other sets were oven cured for 36 h at the range of 40–90 °C and then water cured at room temperature until 7 and 28 days. To build the model, training and testing were conducted by using experimental results from 120 specimens. According to the input parameters in the ANFIS models, the pore volume of each specimen was predicted. The training and testing results in the ANFIS models showed a strong potential for predicting the total specific pore volume of the geopolymeric specimens in the considered range.

Keywords: Geopolymer; Total specific pore volume; Fly ash; Rice husk bark ash; ANFIS

1. Introduction

Although the porous ceramics previously developed by several researchers, it would be of considerable advantage if such porous ceramics could be prepared by a more environmentally friendly process without the need for firing at high temperatures. Geopolymers are good candidates for this purpose, since they are synthesized and hardened at ambient temperatures by the formation of a framework structure of alkali aluminosilicate gel. The term geopolymer was first proposed by Davidovits [1] to describe inorganic aluminosilicate polymers formed from geological materials, and after that many subsequent studies have been reported [2–5]. The synthesis is generally performed by reaction of an alkali silicate solution with a solid aluminosilicate such as fly ash under alkaline conditions. The microstructure and mechanical properties are found to depend strongly on the chemical compositions of the constituent materials. A review by Duxson et al. [3] indicates a trend towards increased mechanical strength at higher SiO_2/Al_2O_3 ratios and increased porosity at higher H_2O/SiO_2 ratios. They also report that the microstructures of geopolymers change significantly at a SiO_2/Al_2O_3 ratio of about 3. A maximum compressive strength of 70 MPa was observed at a SiO_2/Al_2O_3 ratio of 3.8 [3].

The properties of inorganic polymers depend on both the ratio of Si/Al and the types of the utilized raw material. Fly ash (FA) is recently used as a source material to produce geopolymer because of its suitable chemical composition along with favorable size and shape. Fly ash is a by-product of coal-fired electric power stations. Literature survey specifies that fly ash is primarily composed of SiO_2, Al_2O_3 and Fe_2O_3. Since the quality of fly ash depends on the type and the quality of coal along with the performance of the power plant, difficulties sometimes remain to control its chemical composition. In order to achieve a suitable chemical composition to produce geopolymers, the preferred method is to blend fly ash with another high silica source [6].

Rice husk–bark ash (RHBA) is a solid waste generated by biomass power plants using rice husk and eucalyptus bark as fuel. The power plant company providing RHBA for this research reported that about 450 tonnes/day of RHBA are

* Corresponding author. Tel.: +98 255 2241511.
E-mail address: alinazari84@aut.ac.ir (A. Nazari).

0272-8842/$36.00
doi:10.1016/j.ceramint.2011.12.011

produced and discarded. The major chemical constituent of RHBA is SiO_2 (about 75%) [7,8]. Therefore, blending FA and RHBA can adjust the ratio of Si/Al as required.

Adaptive network-based fuzzy inference systems (ANFIS) are the famous hybrid neuro-fuzzy network for modeling the complex systems [9]. ANFIS incorporates the human-like reasoning style of fuzzy systems through the use of fuzzy sets and a linguistic model consisting of a set of IF–THEN fuzzy rules. The main strength of ANFIS models is that they are universal approximators [9] with the ability to solicit interpretable IF–THEN rules. Nowadays, the artificial intelligence-based techniques like ANFIS [10] have been successfully applied in the engineering applications [11].

As authors' knowledge, there are no works on utilizing a mixture of FA and RHBA with different distributions of particles to produce geopolymers. In addition, application of computer programs like ANFIS to predict the properties of geopolymers has been rarely reported. The aim of this study is to investigate the total specific pore volume of geopolymers produced form FA and RHBA mixture experimentally and presenting suitable model based on ANFIS to predict this property. Pore structure of constructional specimens is a very important property which determine the resistance of the specimen to water diffusion and hence deterioration of the material due to attack of chloride and sulfate ions. Therefore, investigating pore structure of the geopolymers seems necessary. Both FA and RHBA with two different particle size distributions were mixed to produce four classes of geopolymers. In the other words, a seeded mixture of fine and coarse FA and RHBA was used. The total specific pore volume of the produced specimens was investigated after specific times of curing. Totally 120 data of porosimetry tests in different conditions were collected, trained and tested by means of ANFIS. The obtained results were compared by experimental ones to evaluate the software power for predicting the total specific pore volume of the specimens.

2. Experimental procedure

The utilized cementitious materials in this work were FA and RHBA. Their chemical compositions which was acquired by XRF analysis has been illustrated in Table 1. In addition, Fig. 1 shows SEM micrograph of FA and RHBA, respectively. The pozzolanic activity of fly ash is completely proved in the literature. For RHBA, only the related peak to SiO_2 obtained by XRD has been illustrated in Fig. 2. As Fig. 2 shows, the SiO_2 in RHBA is amorphous and hence could contribute to the geopolymerization as an active material. The as-received ashes

Table 1
Chemical composition of FA, RHBA and WG (wt%).

Material	SiO_2	Al_2O_3	Fe_2O_3	CaO	SO_3	Na_2O	Loss on ignition
FA[a]	35.21	23.23	12.36	20.01	2.36	0.36	0.24
RHBA[a]	81.36	0.4	0.12	3.23	0.85	–	3.55
WG	34.21	–	–	–	–	13.11	–

[a] Remarks: SiO_2 and Al_2O_3 in FA and RHBA are reactive.

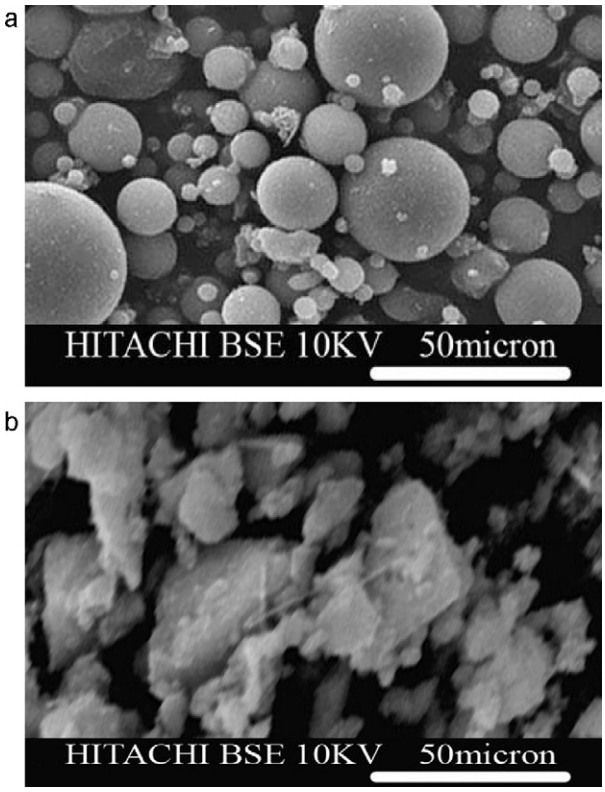

Fig. 1. SEM micrograph of (a) FA and (b) RHBA used in this study.

were sieved and the particles passing the finesses of 150 μm and 33 μm were grinded by using Los Angeles mill for 30 and 180 min, respectively yielded two different samples for each of FA and RHBA. The average particle sizes obtained for FA were 75 μm (coarser FA named cF in this study) and 3 μm (finer FA named fF in this study) with the BET specific surface of 31.3 and 38.9 m^2/g, respectively. The average particle sizes obtained for RHBA were 90 μm (coarser RHBA named cR in this study) and 7 μm (finer RHBA named fR in this study) with the BET specific surface of 26.0 and 33.1 m^2/g, respectively. The four produced samples were used in the experiment. Fig. 3 shows the particle size distribution of the four produced samples.

Sodium silicate solution or water glass (WG) and sodium hydroxide (NaOH) were used as the solution part of the mixture. WG was used without following modification, but the sodium hydroxide was diluted to different concentrations before using. The chemical composition of the utilized WG is also given in Table 1.

Totally 4 series of geopolymer specimens each contains 2 different mixtures of FA and RHBA, as illustrated in Table 2,

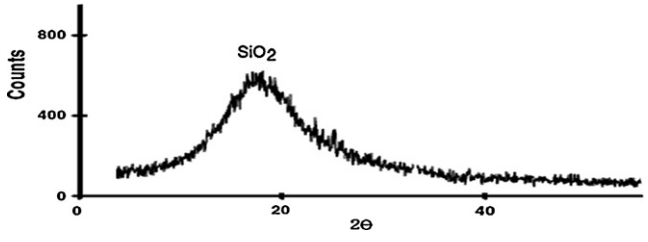

Fig. 2. The related peak to SiO_2 in RHBA.

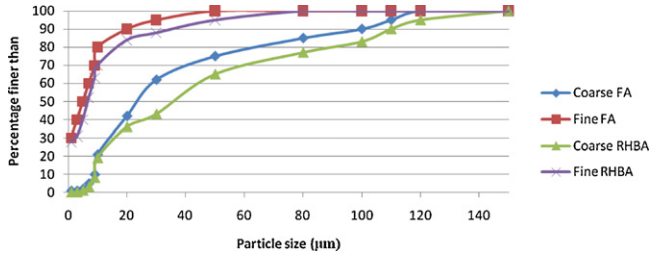

Fig. 3. Particle size distribution pattern of the different ashes used in this study.

were prepared for porosimetry tests. The mixed alkali activator of sodium silicate solution and sodium hydroxide was used. Sodium hydroxide was diluted by tap water to have concentrations of 4, 8 and 12 M. The solution was left under ambient conditions until the excess heat completely dissipated to avoid accelerating the setting of the geopolymeric specimens. Then, the sodium silicate solution was mixed with the sodium hydroxide solution. The ratio of the sodium silicate solution to sodium hydroxide solution was 2.5 by weight for all mixtures because this ratio has been demonstrated the best properties for fly ash-based geopolymers [12,13]. For all samples, the mass ratio of alkali activator to FA-RHA mixture was 0.4. Pastes were mixed by shaking for 5–10 min to give complete homogenization. The mixtures were cast in 30 mm edge polypropylene cubes. The mixing was done in an air-conditioned room at approximately 25 °C. The molds were half-filled, vibrated for 45 s, filled up to the top, again vibrated for 45 s, and sealed with the lid. The mixtures were then precured for 24 h at room temperature. This precuring time has been found to be beneficial to strength development and hence improved properties [14]. Precuring time before application of heat induces significant dissolution of silica and alumina from fly ash and formation of a continuous matrix phase, increasing, therefore, the homogeneity of the geopolymeric materials [14,15]. After the precuring process, the samples and molds were placed in a water bath to prevent moisture loss and the carbonation of the surface. One batch of the samples was placed in an air-conditioned room at 25 °C. The other batch was put in the oven at the elevated temperatures of 50–90 °C for 36 h. To determine the most effective alkali concentration on reduced pore volume, one set of the cured specimens at 80 °C for 36 h were subjected to permeability tests. Afterwards, the other sets were tested at 7 and 28 days of water curing (for the specimens cured in elevated temperature, the time of oven-curing were also considered).

Generally, there are several methods used to measure the pore structure, such as optics method, mercury intrusion porosimetry (MIP), helium flow and gas adsorption [16]. MIP technique is extensively used to characterize the pore structure in porous material as a result of its simplicity, quickness and wide measuring range of pore diameter [16,17]. MIP provides information about the connectivity of pores [16]. In addition, MIP has been shown to produce pore size distribution curves up to three orders of magnitude different from image analysis [18,19].

In this study, the pore structure of concrete is evaluated by using MIP. To prepare the samples for MIP measurement, the concrete specimens after 28 days of curing were first broken into smaller pieces, and then the cement paste fragments selected from the center of prisms were used to measure pore structure. The samples were immersed in acetone to stop hydration as fast as possible. Before mercury intrusion test, the samples were dried in an oven at about 110 °C until constant weight to remove moisture in the pores. MIP is based on the assumption that the non-wetting liquid mercury (the contact angle between mercury and solid is greater than 90°) will only intrude in the pores of porous material under pressure [16,17]. Each pore size is quantitatively determined from the relationship between the volume of intruded mercury and the applied pressure [17]. The relationship between the pore diameter and applied pressure is generally described by Washburn equation as follows [16,17]:

$$D = \frac{-4\gamma \cos\theta}{P} \quad (1)$$

where D is the pore diameter (nm), γ is the surface tension of mercury (dyne/cm), θ is the contact angle between mercury and solid (°) and P is the applied pressure (MPa).

Table 2
Mixture proportioning of the utilized FA and RHBA to produce geopolymeric specimens.

Sample designation	Weight percent of fine FA (fF wt%)	Weight percent of coarse FA (cF wt%)	Weight percent of fine RHBA (fR Wt%)	Weight percent of coarse RHBA (cR Wt%)	SiO_2/Al_2O_3 ratio
fF-fR-1	60	0	40	0	3.81
fF-fR-2	70	0	30	0	2.99
fF-fR-3	80	0	20	0	2.38
fF-cR-1	60	0	0	40	3.81
fF-cR-2	70	0	0	30	2.99
fF-cR-3	80	0	0	20	2.38
cF-fR-1	0	60	40	0	3.81
cF-fR-2	0	70	30	0	2.99
cF-fR-3	0	80	20	0	2.38
cF-cR-1	0	60	0	40	3.81
cF-cR-2	0	70	0	30	2.99
cF-cR-3	0	80	0	20	2.38

Alkali activator (WG + NaOH) to FA-RHBA mixture ratio is 0.4.

Table 3
Total specific pore volume of the geopolymeric specimens (ml/g).

Age of curing	7 days					28 days				
Temperature of oven curing	25 °C	40 °C	60 °C	80 °C	90 °C	25 °C	40 °C	60 °C	80 °C	90 °C
fF-fR-1	0.0354	0.0328	0.0311	0.0294	0.031	0.0283	0.0262	0.0249	0.0235	0.0248
fF-fR-2	0.0338	0.0311	0.0289	0.0269	0.0283	0.027	0.0249	0.0231	0.0215	0.0226
fF-fR-3	0.0349	0.0324	0.0305	0.0285	0.0299	0.0279	0.0259	0.0244	0.0228	0.0239
fF-cR-1	0.0386	0.0357	0.034	0.0321	0.0339	0.0311	0.0288	0.0274	0.0259	0.0273
fF-cR-2	0.0368	0.034	0.0315	0.0294	0.0309	0.0297	0.0274	0.0254	0.0237	0.0249
fF-cR-3	0.0381	0.0353	0.0332	0.0311	0.0326	0.0307	0.0285	0.0268	0.0251	0.0263
cF-fR-1	0.0462	0.0428	0.0408	0.0385	0.0405	0.0364	0.0337	0.0321	0.0303	0.0319
cF-fR-2	0.0441	0.0408	0.0377	0.0352	0.037	0.0347	0.0321	0.0297	0.0277	0.0291
cF-fR-3	0.0456	0.0423	0.0399	0.0373	0.0391	0.0359	0.0333	0.0314	0.0294	0.0308
cF-cR-1	0.0578	0.0535	0.051	0.0481	0.0506	0.0448	0.0415	0.0395	0.0373	0.0392
cF-cR-2	0.0551	0.051	0.0471	0.044	0.0462	0.0427	0.0395	0.0365	0.0341	0.0358
cF-cR-3	0.057	0.0529	0.0498	0.0467	0.0489	0.0442	0.041	0.0386	0.0362	0.0379

Alkali activator (WG + NaOH) to FA-RHBA mixture ratio is 0.4.

The test apparatus used for pore structure measurement is Auto Pore III mercury porosimeter. Mercury density is 13.5335 g/ml. The surface tension of mercury is taken as 485 dynes/cm, and the contact angle selected is 130°. The maximum measuring pressure applied is 200 MPa (30,000 psi), which means that the smallest pore diameter that can be measured reaches about 6 nm (on the assumption that all pores have cylindrical shape). Small samples were used for porosimetry tests.

3. Experimental results and discussion

The total specific pore volume of the produced specimens has been illustrated in Table 3 for 7 and 28 days of curing. Table 3 shows the minimum pore volume has been achieved for fF-fR2 specimen which was oven cured at 80 °C for 36 h in both 7 and 28 days regimes. As Table 3 shows, the optimum curing temperature for all mixtures is 80 °C. Curing temperature has a significant effect on the properties of geopolymers because it affects specimens' setting and hardening. Synthesized products are known to be very sensitive to experimental conditions [20]. However, total specific pore volume begins to increase after curing for a certain period of time at higher temperature. Prolonged curing at higher temperatures can break down the granular structure of geopolymer mixture. This results in dehydration and excessive shrinkage due to contraction of the gel, which does not transform into a more semi-crystalline form [21].

On the whole, samples made with the fine RHBA and FA particles (fF-fR series) showed considerably lower pore volume than the other series. This may be due to production of more compacted specimens. Fine particles are capable to fill the vacancies and produce more densified specimens. This has been confirmed in some works done on concrete specimens [22], but as authors' knowledge there is not any reports confirm this matter in geopolymers.

By comparison the total specific pore volume of the specimens at 7 and 28 days of curing, it is observed that fF-fR series have lower pore volume than the corresponding specimens in fF-cR series. As mentioned above, this is due to more condensed structure of the produced specimens by fine particles. On the other hand, fF-cR series specimens have lower pore volume than the corresponding specimens in cF-fR series. Although fR has been used in cF-fR series, the higher content of cF in these series results in increasing pore volume when compared by the corresponding samples in fF-cR series. Once again, this confirms that the higher content of fine particles would results in the lower pore volume.

4. Architecture of ANFIS

The architecture of an ANFIS model with two input variables has been shown in Fig. 4. Suppose that the rule base of ANFIS contains two fuzzy IF–THEN rules of Takagi and Sugeno's type as follows:

Rule 1: IF x is A_1 and y is B_1, THEN $f_1 = p_1x + q_1y + r_1$.
Rule 2: IF x is A_2 and y is B_2, THEN $f_2 = p_2x + q_2y + r_2$.

Figs. 4 and 5 illustrate fuzzy reasoning and the corresponding equivalent ANFIS architecture, respectively. The functions of each layer are described as follows [9,10,23,24]:

Layer 1 – every node i in this layer is a square node with a node function:

$$O_i^1 = \mu_{A_i}(x) \tag{2}$$

where x is the input to node i and A_i is the linguistic label (fuzzy sets: small, large, etc.) associated with this node function.

Layer 2 – every node in this layer is a circle node labeled P which multiplies the incoming signals and sends the product out. For instance,

$$W_i = \mu_{A_i}(y) \times \mu_{B_i}(y), \quad i = 1, 2 \tag{3}$$

Each node output represents the firing weight of a rule.

Layer 3 – every node in this layer is a circle node labeled N. The ith node calculates the ratio of the ith rule's firing weight to

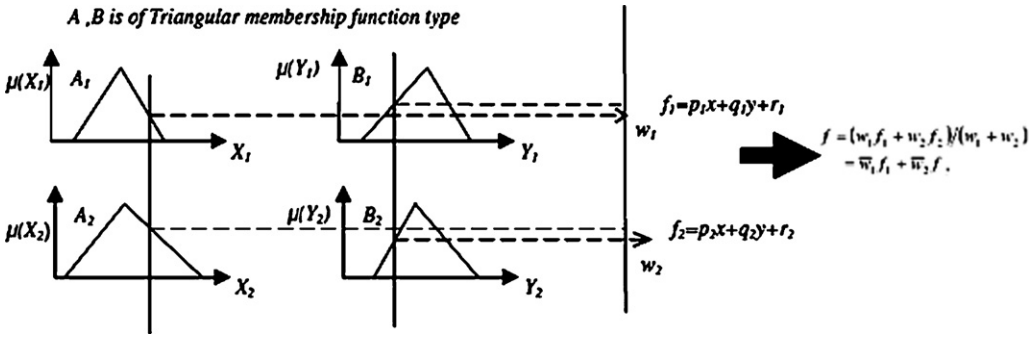

Fig. 4. The reasoning scheme of ANFIS [23].

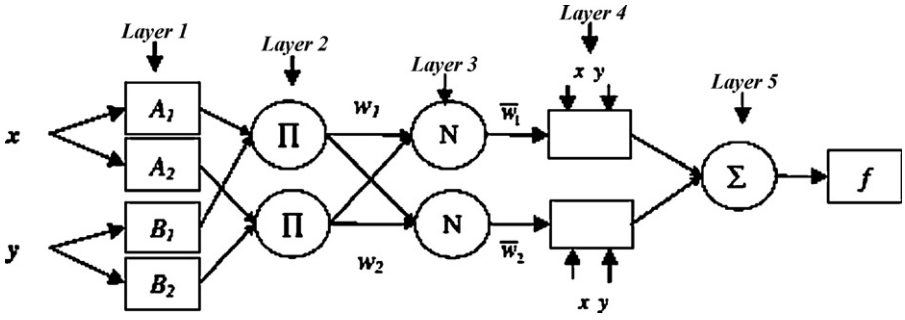

Fig. 5. Schematic of ANFIS architecture [10].

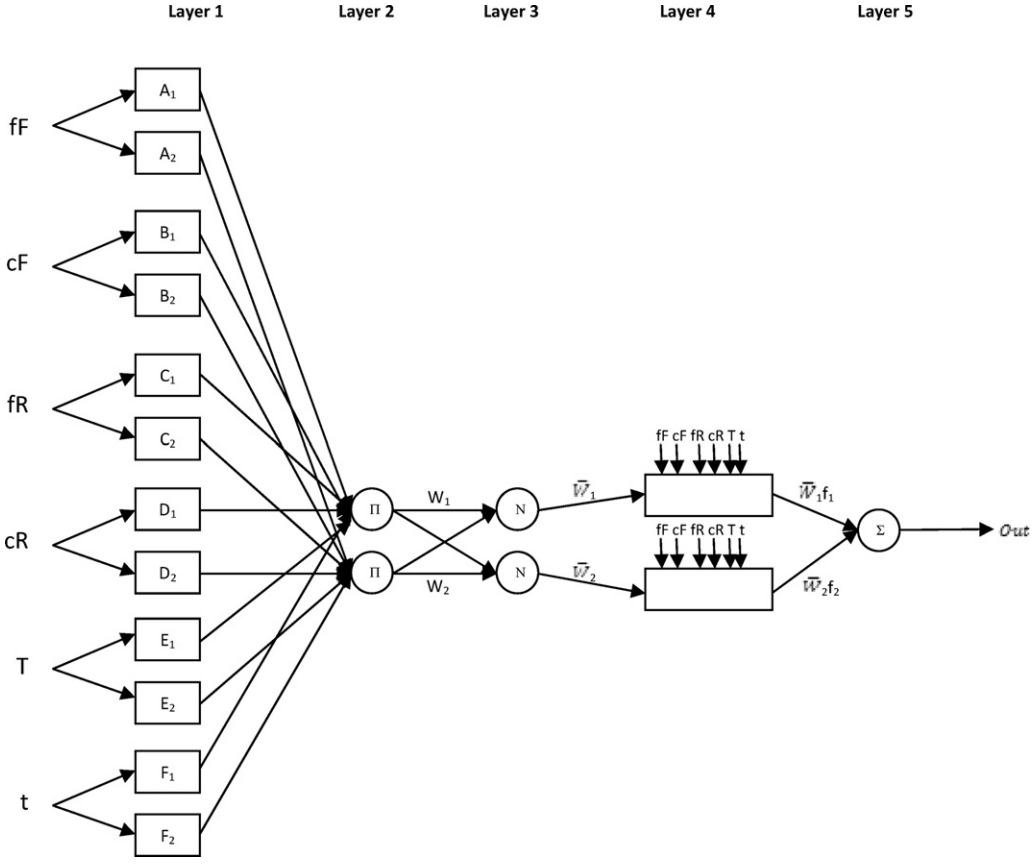

Fig. 6. Schematic of ANFIS architecture utilized in this work.

Table 4
Data sets for comparison of experimental results with results predicted from the ANFIS models.

The percentage of fine fly ash in the ashes mixture (fF)	The percentage of coarse fly ash in the ashes mixture (cF)	The percentage of fine rice husk bark ash in the ashes mixture (fR)	The percentage of coarse rice husk bark ash in the ashes mixture (cR)	The temperature of curing (*T*)	The time of water curing (*t*)	Total specific pore volume values obtained from experiments (ml/g)	Total specific pore volume values predicted by ANFIS-I model (ml/g)	Total specific pore volume values predicted by ANFIS-II model (ml/g)
60	0	40	0	25	7	0.0354	0.0356	0.0342
70	0	30	0	25	7	0.0338	0.0339	0.0336
80	0	20	0	25	7	0.0349	0.0353	0.035
60	0	0	40	25	7	0.0386	0.0385	0.038
70	0	0	30	25	7	0.0368	0.0368	0.0367
80	0	0	20	25	7	0.0381	0.038	0.0381
0	60	40	0	25	7	0.0462	0.0464	0.0461
0	70	30	0	25	7	0.0441	0.0444	0.0444
0	80	20	0	25	7	0.0456	0.044	0.0455
0	60	0	40	25	7	0.0578	0.0554	0.0579
0	70	0	30	25	7	0.0551	0.0573	0.0551
0	80	0	20	25	7	0.057	0.0573	0.0569
60	0	40	0	40	7	0.0328	0.0328	0.0328
70	0	30	0	40	7	0.0311	0.0311	0.0313
80	0	20	0	40	7	0.0324	0.0325	0.0325
60	0	0	40	40	7	0.0357	0.0357	0.0357
70	0	0	30	40	7	0.034	0.0342	0.0347
80	0	0	20	40	7	0.0353	0.0354	0.0353
0	60	40	0	40	7	0.0428	0.0426	0.043
0	70	30	0	40	7	0.0408	0.0409	0.0409
0	80	20	0	40	7	0.0423	0.0416	0.0424
0	60	0	40	40	7	0.0535	0.0536	0.0546
0	70	0	30	40	7	0.051	0.0512	0.0512
0	80	0	20	40	7	0.0529	0.0533	0.0532
60	0	40	0	60	7	0.0311	0.0313	0.031
70	0	30	0	60	7	0.0289	0.0283	0.029
80	0	20	0	60	7	0.0305	0.0312	0.0303
60	0	0	40	60	7	0.034	0.0323	0.0335
70	0	0	30	60	7	0.0315	0.0312	0.0318
80	0	0	20	60	7	0.0332	0.0329	0.0323
0	60	40	0	60	7	0.0408	0.039	0.0392
0	70	30	0	60	7	0.0377	0.0378	0.0372
0	80	20	0	60	7	0.0399	0.0396	0.0389
0	60	0	40	60	7	0.051	0.0503	0.0507
0	70	0	30	60	7	0.0471	0.0458	0.047
0	80	0	20	60	7	0.0498	0.0494	0.0493
60	0	40	0	80	7	0.0294	0.0293	0.0294
70	0	30	0	80	7	0.0269	0.0269	0.0271
80	0	20	0	80	7	0.0285	0.0317	0.0285
60	0	0	40	80	7	0.0321	0.0322	0.0322
70	0	0	30	80	7	0.0294	0.0297	0.0297
80	0	0	20	80	7	0.0311	0.0316	0.0309
0	60	40	0	80	7	0.0385	0.039	0.0384
0	70	30	0	80	7	0.0352	0.0365	0.0355
0	80	20	0	80	7	0.0373	0.0382	0.0373
0	60	0	40	80	7	0.0481	0.0494	0.0483
0	70	0	30	80	7	0.044	0.0452	0.0444
0	80	0	20	80	7	0.0467	0.0477	0.0471
60	0	40	0	90	7	0.031	0.0285	0.031
70	0	30	0	90	7	0.0283	0.0269	0.0282
80	0	20	0	90	7	0.0299	0.0322	0.03
60	0	0	40	90	7	0.0339	0.0339	0.0337
70	0	0	30	90	7	0.0309	0.0308	0.0314
80	0	0	20	90	7	0.0326	0.0323	0.0328
0	60	40	0	90	7	0.0405	0.0402	0.041
0	70	30	0	90	7	0.037	0.0376	0.0375
0	80	20	0	90	7	0.0391	0.0388	0.0391
0	60	0	40	90	7	0.0506	0.0504	0.0496
0	70	0	30	90	7	0.0462	0.0465	0.0459
0	80	0	20	90	7	0.0489	0.0478	0.0487

Table 4 (*Continued*)

The percentage of fine fly ash in the ashes mixture (fF)	The percentage of coarse fly ash in the ashes mixture (cF)	The percentage of fine rice husk bark ash in the ashes mixture (fR)	The percentage of coarse rice husk bark ash in the ashes mixture (cR)	The temperature of curing (*T*)	The time of water curing (*t*)	Total specific pore volume values obtained from experiments (ml/g)	Total specific pore volume values predicted by ANFIS-I model (ml/g)	Total specific pore volume values predicted by ANFIS-II model (ml/g)
60	0	40	0	25	28	0.0283	0.0283	0.0283
70	0	30	0	25	28	0.027	0.0271	0.0271
80	0	20	0	25	28	0.0279	0.0279	0.0278
60	0	0	40	25	28	0.0311	0.031	0.0311
70	0	0	30	25	28	0.0297	0.0296	0.0293
80	0	0	20	25	28	0.0307	0.0308	0.0307
0	60	40	0	25	28	0.0364	0.0365	0.0372
0	70	30	0	25	28	0.0347	0.0349	0.0358
0	80	20	0	25	28	0.0359	0.0373	0.0358
0	60	0	40	25	28	0.0448	0.0448	0.0448
0	70	0	30	25	28	0.0427	0.0427	0.0427
0	80	0	20	25	28	0.0442	0.0461	0.0441
60	0	40	0	40	28	0.0262	0.0266	0.0263
70	0	30	0	40	28	0.0249	0.0253	0.0248
80	0	20	0	40	28	0.0259	0.0261	0.0261
60	0	0	40	40	28	0.0288	0.029	0.029
70	0	0	30	40	28	0.0274	0.0275	0.0273
80	0	0	20	40	28	0.0285	0.0286	0.0288
0	60	40	0	40	28	0.0337	0.0338	0.034
0	70	30	0	40	28	0.0321	0.0321	0.0323
0	80	20	0	40	28	0.0333	0.0348	0.0334
0	60	0	40	40	28	0.0415	0.0439	0.0422
0	70	0	30	40	28	0.0395	0.0397	0.0397
0	80	0	20	40	28	0.041	0.0419	0.0413
60	0	40	0	60	28	0.0249	0.0251	0.0248
70	0	30	0	60	28	0.0231	0.0231	0.023
80	0	20	0	60	28	0.0244	0.0242	0.0244
60	0	0	40	60	28	0.0274	0.0271	0.0272
70	0	0	30	60	28	0.0254	0.0253	0.0256
80	0	0	20	60	28	0.0268	0.0265	0.0268
0	60	40	0	60	28	0.0321	0.0323	0.0322
0	70	30	0	60	28	0.0297	0.0309	0.0295
0	80	20	0	60	28	0.0314	0.0312	0.0313
0	60	0	40	60	28	0.0395	0.0395	0.0394
0	70	0	30	60	28	0.0365	0.0362	0.0365
0	80	0	20	60	28	0.0386	0.0386	0.0383
60	0	40	0	80	28	0.0235	0.0235	0.0237
70	0	30	0	80	28	0.0215	0.022	0.0221
80	0	20	0	80	28	0.0228	0.0231	0.0228
60	0	0	40	80	28	0.0259	0.0265	0.0258
70	0	0	30	80	28	0.0237	0.0239	0.0241
80	0	0	20	80	28	0.0251	0.0255	0.0247
0	60	40	0	80	28	0.0303	0.0324	0.0303
0	70	30	0	80	28	0.0277	0.03	0.0277
0	80	20	0	80	28	0.0294	0.03	0.0297
0	60	0	40	80	28	0.0373	0.0376	0.0375
0	70	0	30	80	28	0.0341	0.0352	0.0338
0	80	0	20	80	28	0.0362	0.037	0.0364
60	0	40	0	90	28	0.0248	0.023	0.0248
70	0	30	0	90	28	0.0226	0.0225	0.0238
80	0	20	0	90	28	0.0239	0.0238	0.0242
60	0	0	40	90	28	0.0273	0.027	0.0275
70	0	0	30	90	28	0.0249	0.0242	0.0255
80	0	0	20	90	28	0.0263	0.0261	0.0263
0	60	40	0	90	28	0.0319	0.032	0.0304
0	70	30	0	90	28	0.0291	0.0294	0.0281
0	80	20	0	90	28	0.0308	0.0304	0.0306
0	60	0	40	90	28	0.0392	0.0388	0.0392
0	70	0	30	90	28	0.0358	0.0362	0.0352
0	80	0	20	90	28	0.0379	0.0372	0.038

the sum of all rule's firing weights:

$$W_i = \frac{W_i}{W_1/W_2}, \quad i = 1, 2 \tag{4}$$

Layer 4 – every node in this layer is a square node with a node function:

$$O_i^4 = \bar{w}_i(p_i x + q_i y + r_1) \tag{5}$$

where $\bar{w}_i$ is the output of layer 3, and $\{p_i, q_i, r_i\}$ is the parameter set.

Layer 5 – the signal node in this layer is a circle node labeled R that computes the overall output as the summation of all incoming signals, i.e.,

$$O_i^5 = \sum_i \bar{w}_i f_i = \frac{\sum_i w_i f_i}{\sum_i w_i} \tag{6}$$

The basic learning rule of ANFIS is the back-propagation gradient descent which calculates error signals recursively from the output layer backward to the input nodes. This learning rule is exactly the same as the back-propagation learning rule used in the common feed-forward neural networks [25,26]. Recently, ANFIS adopted a rapid learning method named as hybrid-learning method which utilizes the gradient descent and the least-squares method to find a feasible set of antecedent and consequent parameters [25,26]. Thus in this paper, the later method is used for constructing the proposed models.

4.1. ANFIS model structure and parameters

The structure of the proposed ANFIS networks is consisted of six input variables including the percentage of fine fly ash in the ashes mixture (fF), the percentage of coarse fly ash in the ashes mixture (cF), the percentage of fine rice husk bark ash in the ashes mixture (fR), the percentage of coarse rice husk bark ash in the ashes mixture (cR), the temperature of curing (T) and the time of water curing (7 or 28 days) (t). The value for the output layer is the total specific pore volume (TSPV). The input space is decomposed by three fuzzy labels. In this paper, for comparison purposes, two types of membership functions (MFs) including the triangular (ANFIS-I) and Gaussian (ANFIS-II) were utilized to construct the suggested models. The ANFIS models were trained by 94 input–target pairs and tested by 26 data from testing data. Moreover, up to 1000 epochs were specified for training process to assure the gaining of the minimum error tolerance.

Matlab ANFIS toolbox was used for ANFIS applications. To overcome optimization difficulty, a program has been developed in Matlab which handles the trial and error process automatically [27–30].

The IF-THEN rules in this study were achieved as follows. Suppose that the rule base of ANFIS contains two fuzzy IF–THEN rules of Takagi and Sugeno's type:

Rule 1: IF fF is A_1, cF is B_1, fR is C_1, cR is D_1, T is E_1 and t is F_1 THEN $f_1 = p_1\text{fF} + q_1\text{cF} + r_1\text{fR} + s_1\text{cR} + t_1 T + u_1 t + v_1$.

Rule 2: IF fF is A_2, cF is B_2, fR is C_2, cR is D_2, T is E_2 and t is F_2 THEN $f_2 = p_2\text{fF} + q_2\text{cF} + r_2\text{fR} + s_2\text{cR} + t_2 T + u_2 t + v_2$.

The corresponding equivalent ANFIS architecture is shown in Fig. 6. The functions of each layer are described as follows:

Layer 1 – every node i in this layer is a square node with a node function:

$$O_i^1 = \mu_{A_i}(\text{fF}), \quad i = 1, 2 \tag{7}$$

$$O_i^1 = \mu_{B_i}(\text{cF}), \quad i = 1, 2 \tag{8}$$

$$O_i^1 = \mu_{C_i}(\text{fR}), \quad i = 1, 2 \tag{9}$$

$$O_i^1 = \mu_{D_i}(\text{cR}), \quad i = 1, 2 \tag{10}$$

$$O_i^1 = \mu_{E_i}(T), \quad i = 1, 2 \tag{11}$$

$$O_i^1 = \mu_{F_i}(t), \quad i = 1, 2 \tag{12}$$

where fF, cF, fR, cR, T and t are inputs to node i, and A_i, B_i, C_i, D_i, E_i and F_i are the linguistic label (fuzzy sets: small, large, etc.) associated with this node function.

Layer 2 – every node in this layer is a circle node labeled Π which multiplies the incoming signals and sends the product out:

$$W_i = \mu_{A_i}(\text{fF}) \times \mu_{B_i}(\text{cF}) \times \mu_{C_i}(\text{fR}) \times \mu_{D_i}(\text{cR}) \times \mu_{E_i}(T) \times \mu_{F_i}(t), \quad i = 1, 2 \tag{13}$$

Each node output represents the firing weight of a rule.

Layer 3 – every node in this layer is a circle node labeled N. The ith node calculates the ratio of the ith rule's firing weight to the sum of all rule's firing weights:

$$W_i = \frac{W_i}{W_1/W_2}, \quad i = 1, 2 \tag{14}$$

Layer 4 – every node in this layer is a square node with a node function:

$$O_i^4 = \bar{w}_i(P_i\text{fF} + q_i\text{cF} + r_i\text{fR} + s_i\text{cR} + t_i T + u_i t + v_i) \tag{15}$$

where $\bar{w}$ is the output of layer 3, and $\{p_i, q_i, r_i, s_i, t_i, u_i, v_i, z_i\}$ is the parameter set.

Layer 5 – the signal node in this layer is a circle node labeled R that computes the overall output as the summation of all incoming signals, i.e.,

$$O_i^5 = \sum_i \bar{w}_i f_i = \frac{\sum_i w_i f_i}{\sum_i w_i} \tag{16}$$

5. Predicted results and discussion

In this study, the error arose during the training and testing in ANFIS-I and ANFIS-II models can be expressed as

absolute fraction of variance (R^2) which are calculated by Eq. (17) [31]:

$$R^2 = 1 - \left(\frac{\sum_i (t_i - o_i)^2}{\sum_i (o_i)^2} \right) \quad (17)$$

where t is the target value and o is the output value.

All of the results obtained from experimental studies together with those predicted by training and testing phases of ANFIS-I and ANFIS-II models are given in Fig. 7a and b, respectively. The linear least square fit line, its equation and the R^2 values have been shown in these figures for the training and testing sets. Also, inputs values and experimental results with training and testing results obtained from ANFIS-I and ANFIS-II models have been given in Table 4. As it is visible in Fig. 7, the values obtained from the training and testing in ANFIS-I and ANFIS-II models are very close to the experimental results. The result of testing phase in Fig. 7 shows that ANFIS-I and ANFIS-II models are capable of generalizing between input and output variables with reasonably good predictions.

The performance of the ANFIS-I and ANFIS-II models has been shown in Fig. 7. The best value of R^2 is 99.76% for training set in the ANFIS-II model. The minimum value of R^2 is 98.68% for testing set in the ANFIS-I model. All of R^2 values show that the proposed ANFIS-I and ANFIS-II models are suitable and can predict the total specific pore volume values very close to the experimental ones. Finally it should be stated that ANFIS prediction of pore structure has been trained using MIP data and a strong correlation has been obtained. However, comparing ANFIS predictions with image analysis results is likely to show discrepancies because MIP and image analysis results do not produce consistent results.

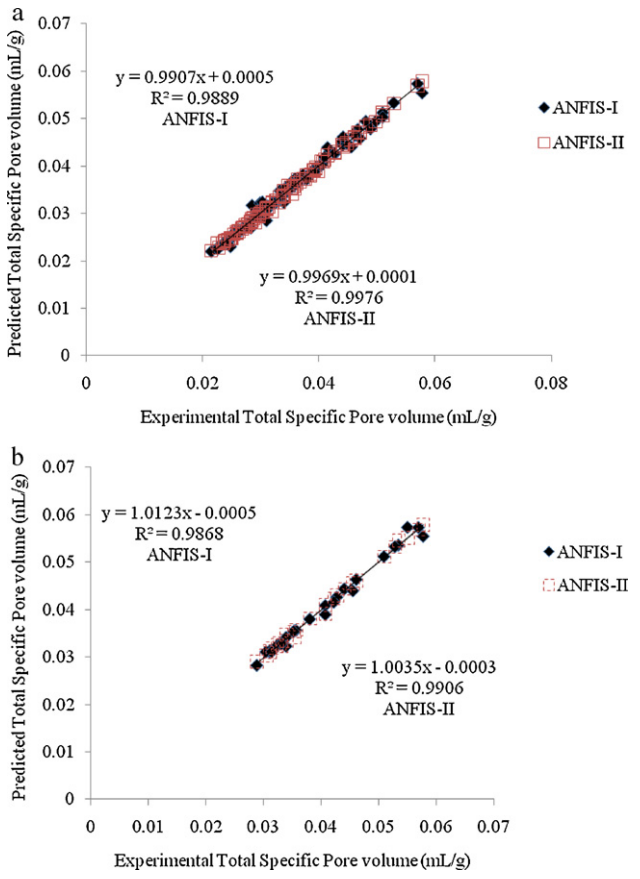

Fig. 7. The correlation of the measured and predicted total specific pore volume values of geopolymers in (a) training and (b) testing phase for ANFIS models.

6. Conclusions

From the experimental procedure and ANFIS modeling, the following results were obtained:

1. The total specific pore volume of the specimens depends on the particle size distribution pattern of the ashes, the time of oven curing and the time of room curing. The finer the ashes particle size results in the denser paste and hence the reduced pore volume in the specimens. On the other hand, oven curing of the specimens at 80 °C was found to be the optimum condition of curing in geopolymeric specimens.
2. In all mixtures, the specimens with the SiO_2/Al_2O_3 ratio equal to 2.99 had the lowest pore volume. In the other words, the lowest pore volume was achieved for the mixture of fine fly ash to fine rice husk bark ash of 70:30.
3. ANFIS can be an alternative approach for evaluation the effect of utilization a seeded mixture of FA and RHBA on total specific pore volume values of geopolymer specimens.
4. Comparison between ANFIS models in terms of R^2 showed that ANFIS models are capable to predict suitable results for pore volume values of geopolymer specimens.

References

[1] J. Davidovits, Inorganic polymeric new materials, J. Therm. Anal. Calorim. 37 (1991) 1633–1656.
[2] V.F.F. Barbosa, K.J.D. MacKenzie, Synthesis and thermal behavior of potassium sialate geopolymers, Mater. Lett. 57 (2003) 1477–1482.
[3] P. Duxson, J.L. Provis, G.C. Lukey, S.W. Mallicoat, W.M. Kriven, J.S.J. van Deventer, Understanding the relationship between geopolymer composition, microstructure and mechanical properties, Colloids Surf. 269 (2005) 47–58.
[4] P. Duxson, A. Fernandez-Jimenez, J.L. Provis, G.C. Lukey, A. Palomo, J.S.J. van Deventer, Geopolymer technology: the current state of the art, J. Mater. Sci. 42 (2007) 2917–2933.
[5] C. Panagiotopoulou, E. Kontori, T. Perraki, G. Kakali, Dissolution of aluminosilicate minerals and by-products in alkaline media, J. Mater. Sci. 42 (2007) 2967–2973.
[6] J. Wongpa, K. Kiattikomol, C. Jaturapitakkul, P. Chindaprasirt, Compressive strength, modulus of elasticity, and water permeability of inorganic polymer concrete, Mater. Des. 31 (2010) 4748–4754.
[7] V. Sata, C. Jaturapitakkul, K. Kiattikomol, Influence of pozzolan from various byproduct materials on mechanical properties of high-strength concrete, Constr. Build. Mater. 21 (7) (2007) 1589–1598.
[8] W. Tangchirapat, R. Buranasing, C. Jaturapitakkul, P. Chindaprasirt, Influence of rice husk–bark ash on mechanical properties of concrete containing high amount of recycled aggregates, Constr. Build. Mater. 22 (8) (2008) 1812–1819.
[9] J.S.R. Jang, ANFIS: adaptive-network-based fuzzy inference system, IEEE Trans. Syst. Man Cyber 23 (3) (1993) 665–685.
[10] M. Sarıdemir, Predicting the compressive strength of mortars containing metakaolin by artificial neural networks and fuzzy logic, Adv. Eng. Soft 40 (9) (2009) 920–927.

[11] A. Nazari, N. Didehvar, Modeling impact resistance of aluminum-epoxy laminated composites by ANFIS, Compos. Part B: Eng. 42 (2011) 1912–1919.
[12] F. Pacheco-Togal, J. Castro-Gomes, S. Jalali, Investigation about the effect of aggregates on strength and microstructure of geopolymeric mine waste mud binders, Cement Concrete Res. 37 (6) (2007) 933–941.
[13] F. Pacheco-Torgal, J.P. Castro-Gomes, S. Jalali, Studies about mix composition of alkali-activated mortars using waste mud from Panasqueira, in: Proceedings of the Engineering Conference, University of Beira Interior, Covilha, Portugal, 2005.
[14] T. Bakharev, Geopolymeric materials prepared using Class F fly ash and elevated temperature curing, Cement Concrete Res. 35 (2005) 1224–1232.
[15] P. Chindaprasirt, T. Chareerat, V. Sirivivatnanon, Workability and strength of coarse high calcium fly ash geopolymer, Cement Concrete Comp. 29 (2007) 224–229.
[16] A.B. Abell, K.L. Willis, D.A. Lange, Mercury intrusion porosimetry and image analysis of cement-based materials, J. Colloid Interface Sci. 211 (1999) 39–44.
[17] K. Tanaka, K. Kurumisawa, Development of technique for observing pores in hardened cement paste, Cement Concrete Res. 32 (2002) 1435–1441.
[18] D.A. Lange, H.M. Jennings, S.P. Shah, Image analysis techniques for characterization of pore structure of cement-based materials, Cement Concrete Res. 24 (5) (1994) 841–853.
[19] D.L.Y. Kong, J.G. Sanjayan, K. Sagoe-Crentsil, Comparative performance of geopolymers made with metakaolin and fly ash after exposure to elevated temperatures, Cement Concrete Res. 37 (2007) 1583–1589.
[20] A. Fernandez-Jimenez, I. Garcia-Lodeiro, A. Palomo, Durability of alkali-activated fly ash cementitious materials, J. Mater. Sci. 42 (9) (2007) 3055–3065.
[21] J.G.S. Van Jaarsveld, J.S.J. Van Deventer, G.C. Lukey, The effect of composition and temperature on the properties of fly ash—and kaolinite-based geopolymers, Chem. Eng. J. 89 (1–3) (2002) 63–73.
[22] A. Naji Givi, S. Abdul Rashid, F. Nora, A. Aziz, M.A. Mohd Salleh, Assessment of the effects of rice husk ash particle size on strength, water permeability and workability of binary blended concrete, Constr. Build. Mater. 24 (11) (2010) 2145–2150.
[23] A.A. Ramezanianpour, M. Sobhani, J. Sobhani, Application of network based neuro-fuzzy system for prediction of the strength of high strength concrete, Amirkabir J. Sci. Technol. 5 (59-C) (2004) 78–93.
[24] A.A. Ramezanianpour, J. Sobhani, M. Sobhani, Application of an adaptive neurofuzzy system in the prediction of HPC compressive strength, in: Proceedings of the Fourth International Conference on Engineering Computational Technology, Civil-Comp Press, Lisbon, Portugal, 2004, p. 138.
[25] I.B. Topcu, M. Sarıdemir, Prediction of mechanical properties of recycled aggregate concretes containing silica fume using artificial neural networks and fuzzy logic, Compos. Mater. Sci. 42 (1) (2008) 74–82.
[26] J.S.R. Jang, C.T. Sun, Nuro-fuzzy modeling and control, Proc. IEEE 83 (3) (1995).
[27] I.H. Guzelbey, A. Cevik, A. Erklig, Prediction of web crippling strength of cold-formed steel sheetings using neural networks, J. Constr. Steel Res. 62 (2006) 962–973.
[28] I.H. Guzelbey, A. Cevik, M.T. Gögüs, Prediction of rotation capacity of wide flange beams using neural networks, J. Constr. Steel Res. 62 (2006) 950–961.
[29] A. Cevik, I.H. Guzelbey, Neural network modeling of strength enhancement for Cfrp confined concrete cylinders, Build. Environ. 43 (2008) 751–763.
[30] A. Cevik, I.H. Guzelbey, A soft computing based approach for the prediction of ultimate strength of metal plates in compression, Eng. Struct. 29 (3) (2007) 383–394.
[31] I.B. Topcu, M. Sarıdemir, Prediction of compressive strength of concrete containing fly ash using artificial neural network and fuzzy logic, Compos. Mater. Sci. 41 (3) (2008) 305–311.